Direct numerical simulation of igniting non-premixed hydrogen combustion for the Argon Power Cycle

Quan Reyes, D. A.; Roekaerts, Dirk; van Oijen, Jeroen

DOI
10.1016/j.proci.2024.105553

Publication date
2024

Document Version
Final published version

Published in
Proceedings of the Combustion Institute

Proceedings of the Combustion Institute 40 (2024) 105553

Contents lists available at ScienceDirect

Proceedings of the Combustion Institute

journal homepage: www.elsevier.com/locate/proci

Direct numerical simulation of igniting non-premixed hydrogen combustion for the Argon Power Cycle

D.A. Quan Reyes [a,*], Dirk Roekaerts [b], Jeroen van Oijen [a]

[a] Power and Flow, Mechanical Engineering, TU Eindhoven, Eindhoven, The Netherlands
[b] Department of Process & Energy, TU Delft, Delft, The Netherlands

ARTICLE INFO

Keywords:
Hydrogen
DNS
Non-premixed
FGM

ABSTRACT

The Argon Power Cycle (APC) is a compression ignition combustion concept that would substantially enhance efficiency by using argon as the working fluid. When used with hydrogen and oxygen, such closed loop system would be free of emissions. Fundamental understanding on the combustion dynamics of such system is needed in order to determine the best injection strategy. A direct numerical simulation of a fully developed turbulent (Re = 10 000) reacting case which resembles the direct injection of H_2 has been performed. Attention was devoted to (1) understanding the influence of preferential diffusion and turbulence on the ignition behavior and development of flame kernels, (2) determining the composition space accessed by the turbulent and laminar analogue, and (3) finding the types of flamelets that could resemble such composition space. It was found that igniting kernels emerge near the stoichiometric mixture fraction in regions convex to the fuel side, and with high scalar dissipation, in contrast to what has been reported for other fuels in the literature. Furthermore, these igniting kernels can extinguish if exposed to high curvature levels due to the enhanced diffusion of radicals out of the kernel. There is good agreement between the composition space accessed by the turbulent flame and the laminar analogue, but better agreement can be reached by using strained and curved flamelets.

1. Introduction

According to the United Nations Environment Program's latest report [1], continuing with current climate policies and emissions will result in an average global warming of 3°C during this century, with a 66% chance. Besides the social and political challenges, technical solutions to replace fossil fuels are paramount, and clean hydrogen combustion could contribute to this end.

The Argon Power Cycle (APC) is a novel combustion technology that relies on the use of Ar as the working fluid. When such system is used with H_2 and O_2, the exhaust would be free of emissions and effectively contains only water and argon, which allows for easy separation. The highest efficiency of such system would be achieved operating at high-pressure, hence a major challenge is to adequately control the injection of fuel at such conditions. To that end, sound understanding the combustion nature is needed, and the standard models used in the context of coarse scale simulations methods, e.g. Reynolds Average Navier Stokes (RANS) or Large Eddy Simulations (LES) are not ensured to be readily applicable, since they rely on closure models which might not apply to H_2, as some of its physical properties largely differ from traditional fuels.

Direct numerical simulations (DNS) with detailed chemistry can help acquire such fundamental understanding to levels that are unfeasible by experimental techniques, at moderate Reynolds numbers (Re). In a DNS, all relevant temporal and spatial scales are resolved, which provide information to create accurate sub-models for the large-scale studies.

Here, a DNS resembling the injection of pure H_2 in a mixture of Ar + O_2 and is computed with detailed chemistry and accurate expressions for diffusion and viscosity, to better understand the nature of the ignition, combustion, and its modeling via flamelets. The case is computed at Re = 10 000, which according to [2], is the minimum value to have fully developed turbulence. This work is structured in the following sections, (1) introduction (2) numerical configuration, (3) the influence of turbulence and preferential diffusion on ignition, (4) composition space of laminar and turbulent flames, (5) considerations for flamelet-based modeling, and (6) conclusions.

2. Numerical configuration

2.1. Direct numerical simulation of turbulent case

The DNS consists of a temporal, planar, double-shear layer that is computed using an in-house code named Disco, based on the compact

* Corresponding author.
E-mail address: d.a.quan.reyes@tue.nl (D.A. Quan Reyes).

https://doi.org/10.1016/j.proci.2024.105553
Received 4 December 2023; Accepted 29 June 2024
Available online 2 August 2024

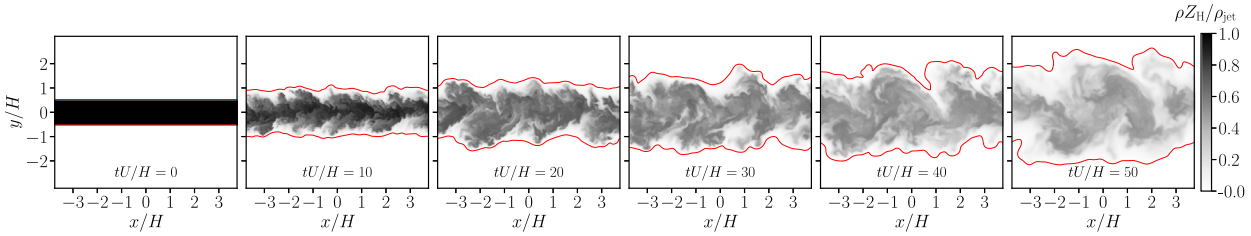

Fig. 1. Evolution of normalized ρZ_H. The red line depicts $Z = Z_{st}$. (For interpretation of the references to color in this figure legend, the reader is referred to the web version of this article.)

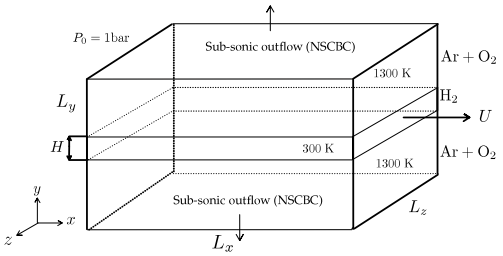

Fig. 2. Schematic of the DNS configuration.

Table 1
DNS parameters.

Description	Value
Jet speed (U)	565 m s^{-1}
Turbulence intensity u'_{rms}/U	10%
Jet height (H)	1.99 mm
Domain size (L_x, L_y, L_z)	(1.5, 1.25, 0.75) cm
Grid size (Δx)	12.5 μm
Fuel temperature (T_{fuel})	300 K
Oxidizer temperature (T_{ox})	K
Oxidizer composition	$X_{Ar} : X_{O_2} = 9 : 1$

finite difference scheme derived in [3]. This scheme is 5th order accurate for the acoustic and advective terms, and 6th order for the diffusive terms. Time integration is performed using an explicit, 3rd order Runge–Kutta scheme. The evolution of hydrogen element mass (ρZ_H), is depicted in Fig. 1, where ρ is the local density, Z_H is the hydrogen element-based mass fraction, and ρ_{jet}, is the initial jet density. A schematic representation of the system is shown in Fig. 2. Table 1 presents the parameters of the DNS configuration.

The code solves for the fully compressible Navier–Stokes equations. Diffusion is modeled using non-unity Lewis numbers (Le_α) to include preferential diffusion. Viscosity is computed using the momentum-averaged mixing rules [4], which show a maximum difference of 2% with respect to the multi-component model developed in [5], in a one-dimensional (1D) binary mixing problem of H_2 + Ar. The chemical source terms are computed with the chemical mechanism derived by Burke et al. [6] with 9 species and 21 reactions. The reader is referred to [7] for details on the equations solved.

The domain consists of a box of size $(1.5 \times 1.25 \times 0.75)$ cm^3 with mesh spacing $\Delta x = 12.5$ μm. The boundary conditions are periodic in the x, z directions, and sub-sonic outflow in the y direction. These subsonic boundaries are implemented as per [8], which differ from the original formulation [9] in such that these include treatment for transverse terms with a relaxation factor as a function of the local Mach number (Ma), as well as chemical source-terms, to prevent non-orthogonal reflection as reported in [10] and spurious waves when reactions take place near the boundaries [11].

The streams consist of a jet of pure H_2 surrounded by a mixture of Ar + O_2 at an expected operating temperature of 1300 K. The domain pressure is 1 bar since the focus here is on turbulence-chemistry interaction, the effect of pressure shall be studied elsewhere. The initial profiles for species, temperature and density are defined using a hyperbolic tangent of thickness $\delta_y = 1$ μm, i.e. $f \propto \tanh(y/\delta_y)/2 + 0.5$. This profile is then integrated in time for 1 μs without chemical reactions, to allow preferential diffusion effects to reach an equilibrium between species before it is applied to the DNS. The pure H_2 jet of thickness $H = 1.99$ mm is traveling at a speed of $U = 565$ m s^{-1} for $Re = 10\,000$. Isotropic turbulence with a root-mean-square (rms) intensity $I = u'_{rms}/U = 0.1$ is superimposed on the jet by filtering a random noise field. The DNS is computed until a time of 0.201 ms equivalent to $t' = tU/H = 57$, which is sufficient for ignition and steady combustion to take place. Table 2 shows the turbulent quantities for three times of interest at the location of the Kolmogorov length along y i.e., $\min(\eta_y = (\tilde{\nu}_y^3/\tilde{\epsilon}_y)^{1/4})$, where $\tilde{\epsilon}_y = 2\overline{\rho \cdot \nu \langle s_{ij} \rangle}/\bar{\rho}$ averaged in x, z, ν is the kinematic viscosity and $\langle s_{ij} \rangle$ is the dot-product of the strain rate tensor with itself. It can be seen that the Kolmogorov scale is well resolved. Fig. 1 shows the evolution of normalized elemental hydrogen mass at the middle z-plane. From this figure it is possible to see the transition to turbulence created by the shearing forces and that the stoichiometric mixture fraction (Z_{st}) remains on the outer edge of the turbulent layer.

Table 2
Turbulent quantities.

t'	$\eta/\Delta x$	τ_η [μs]	L_t [mm]	τ_t [μs]	Re_t
30	1.15	1.12	1.37	29.3	688
40	1.64	1.89	1.90	48.8	666
50	2.41	2.77	1.61	49.4	318

3. The influence of preferential diffusion and turbulence on ignition

Ignition is one of the most important phenomena in fuel injection applications, and can be considered to be the chronological starting point of combustion. To this day, many questions remain open regarding what exactly happens at the smallest scale during an ignition process. Even in chemically 'simple' fuels like hydrogen, predicting ignition accurately in certain conditions, like low temperature ($T <$ 1000 K) is troublesome, experimentally or with detailed chemistry modeling as seen in, e.g. [6,12–14], and it continues to be a topic of research.

Mastorakos provided a comprehensive study on the ignition of non-premixed flames [15]. He argues that, in essence, ignition kernels will happen at regions of low scalar dissipation ($\chi = 2D\left(\partial Z/\partial x_i\right)^2$), where $D = \lambda/(\rho c_p)$, as these regions will have lower diffusion of radicals away from the pool, thus allowing the run off behavior. He also argues that, in general, turbulent flames will have longer ignition delay compared to their counter part due to the enhanced scalar dissipation created by the turbulence. However, Göktola and van Oijen found the opposite effect, where under certain conditions, turbulence can reduce the ignition delay compared to laminar mixing layers [16,17]. The reason is that turbulence creates a distribution of χ, with some values being lower

Table 3
Ignition delay for the three cases.

Case	Ignition delay [s]	Ratio
$1D_{Le}$	86.5 μs	
$1D_{\text{Unity}}$	161.5 μs	1.87
$3D_{Le}$	108.5 μs	1.25

than the laminar analogue, thus allowing for faster ignition. Mastorakos proposed that the best method to determine the most reactive mixture fraction (Z_{mr}) is by igniting laminar mixing layers. This method is used here, with focus on the point where maximum source term ω_{HO_2} takes place, as it is a indicator of preignition [18]. The result is $Z_{\text{mr}} = 8.2 \times 10^{-3}$, while $Z_{\text{st}} = 10.1 \times 10^{-3}$, which are very close, in contrast to what is found for other fuels [15].

3.1. Effect of preferential diffusion on the ignition

Two systems are investigated to assess the effect of preferential diffusion, a laminar mixing layer and a turbulent mixing initialized with the profiles described in the section above. The first is computed with two diffusion models based on $Le = 1$ and $Le_\alpha \neq 1$, named $1D_{\text{Unity}}$ and $1D_{Le}$, respectively. The turbulent system is named $3D_{Le}$. Ignition delay is defined as the time where Y_H is 50% of maximum. The resulting ignition delays can be seen in Table 3. It is clear that the preferential diffusion reduces the ignition delay compared to $Le = 1$. The low value of Le_H, Le_{H_2}, results in fast diffusion of H and H_2 into the oxidizer side, resulting in mixtures which are more prone to ignite [7]. The ignition delay of the turbulent case is 25% slower than the laminar mixing layer.

3.2. Effect of turbulence on the igniting kernels

The focus of this section is on the development of the igniting kernels and how these are affected by turbulence. The emergence of kernels is qualitatively clear from $t' > 32$, so that is chosen as the starting point. Fig. 3 depicts the evolution of the following key variables $\chi, Y_H, \omega_H, Y_{H_2O}, Y_{H_2}, Y_{O_2}$. The relevance of χ was already mentioned. Y_H is key for the pathway from ignition to steady combustion, Y_{H_2O} provides information on the overall progress of reaction, and Y_{H_2} and Y_{O_2} are the reactants. The dashed line shows $Z = Z_{\text{st}}$.

The main findings are summarized in the following:

- In Fig. 3, at $t' = 32$, the ignition kernels arise near $Z = Z_{\text{st}}$ in the regions convex to the fuel side (positive curvature) and not necessarily at those with low values of χ, in contrast to what has been reported in the literature. Actually, the opposite can be seen where the locations of ignition kernel formations correspond to regions of high χ. These are located slightly shifted into the fuel side with respect to $Y_H, \omega_H, \omega_{H_2O}$.
- Defining curvature ($\kappa = \nabla \cdot \mathbf{n}$) with $\mathbf{n} = \nabla Z_H / \|\nabla Z_H\|$, and focusing on the kernel located near $(x/H, y/H) = (0, 1)$, clearly identified by a rectangle in the ω_H contours starting at $t' = 32$ and following it in time, it is observed that the increase in curvature of Z_{st} corresponds spatially to increased reaction rates, visible in the behavior of ω_H and ω_{H_2O} at $t' = 40$. However, in the lower part of the kernel, there is also an increase in the negative value of ω_H, which spatially corresponds to a high value of χ. At $t' = 44$ and 48, the kernel of interest has considerably decreased its reactivity up to the point of extinction. Y_H is not increasing as in the other kernels, but it is mostly diffusing. In other words, the curvature can enhance the formation of kernels, but it can also extinguish them.
- Fig. 3 shows that the region where the kernel extinguished still contains reactants, so the extinction was not due to lack of reactants but due to turbulence.

A deeper analysis is made to understand the process of extinction of the igniting kernel at $t' = 38$. To that end, the χ and κ, ω_H and the diffusion term $D_H = \frac{\partial}{\partial x_i}\left(\frac{\lambda}{Le_H c_p}\frac{\partial Y_H}{\partial x_i}\right)$ are studied and shown in Figs. 4(a), 4(b), 4(c) and 4(d), respectively.

From these four figures it is seen that the transition from positive to negative κ correspond to positive and negative diffusion. Also the diffusion and the source term are comparable in magnitude, which can explain why the kernel is extinguishing. From Figs. 4(c) and 4(a), it is possible to see the decrease of Y_H being located at high χ.

Another remarkable feature appears when focusing on Fig. 4(b). Here it is clear that the largest values of curvature are found at the fuel rich side, where turbulence level is highest. Nevertheless, some curvature is visible across the isocontour, characterized by smooth 'corrugations' that cross the Z_{st} isocontours. The regions where these lines cross the reaction zones, are much more reactive (Fig. 4(c)), and much more diffusive (Fig. 4(d)), and do not necessarily correlate spatially to high or low values of χ.

Figs. 5(a), 5(b) display the states inside the box enclosing the kernel region in Fig. 4(c) at the time of preignition and extinction. The scatter represents the 3D case at $t' = 29$ and the line represents the 1D laminar mixing layer at $t' = 24$. The scalar dissipation rate vs Z_H, colored by the balance of the source terms and diffusion is shown. The laminar mixing layer is also shown in 5(b) during preignition and not shown for later stages as the source term of interest has dropped to a maximum of 7.62 kg m^{-3}s^{-1}. From this comparison its possible to see the turbulent case has higher overall production of Y_H at higher χ, concentrated in $Z_H/Z_{\text{st}} < 4$, while the laminar flame has more extended rich zones. Also, in Fig. 5(b), a zone with overall negative rate appears between $2 < Z_H/Z_{\text{st}} < 8$ and $10 < \chi < 200$ s^{-1}, as well as a zone with overall positive rate for richer and higher values of χ, both of which are not present in the laminar flamelet.

4. Composition space of laminar and turbulent mixing layers

The composition space constitutes the thermochemical states that a reacting flow may access during the combustion process, which consists of the mass fractions of all species, temperature and pressure. Flamelet-based tabulated chemistry methods such as the Flamelet-Generated Manifold (FGM) method builds on the idea that ensemble of laminar flamelets can accurately represent the combustion physics of a turbulent flame. And that there is a reduced number of basis vectors that can be used to locally span the surface in composition space formed by the states in the flame. Here we seek to answer the questions: what is the composition space accessed by the 3D DNS? How does this space and the one created by laminar flamelets compare?

FGM, first introduced in [19] has shown to be an accurate approach for a large range of combustion phenomena (e.g. [20–22]). The adequacy of this method depends largely on the types of flamelets used to span the composition space expected to be present in a turbulent flame, and the variables used to parametrize such space. The standard approach to model non-premixed combustion is to use a mixture fraction (related to the mixture space) and a progress variable (related to reaction evolution). Here we define the progress variable as $\mathcal{Y} = Y_{H_2O}$.

To investigate the effect of the turbulence in composition space, discrete joint probability density functions (JPDF) of the $3D_{Le}$ case are computed as functions of Z_H, Y_{H_2O} in a $[100 \times 100]$ matrix. 75 equally spaced z planes from $t' = 38$ are used. This time is representative of the transition from ignition to the quasi-steady burning phase.

Fig. 6(a) depicts the JPDF and it is remarkably similar in scale and distribution compared to the space created by the 1D igniting laminar mixing layer $1D_{Le}$, shown in 6(b), which can be regarded as an FGM. The major difference between these two is that the FGM predicts more progress in the richer zones. This could be due to the fact that the maximum value of Z_H decreases quickly in the turbulent case due to mixing, or that there was not sufficient reaction in that region.

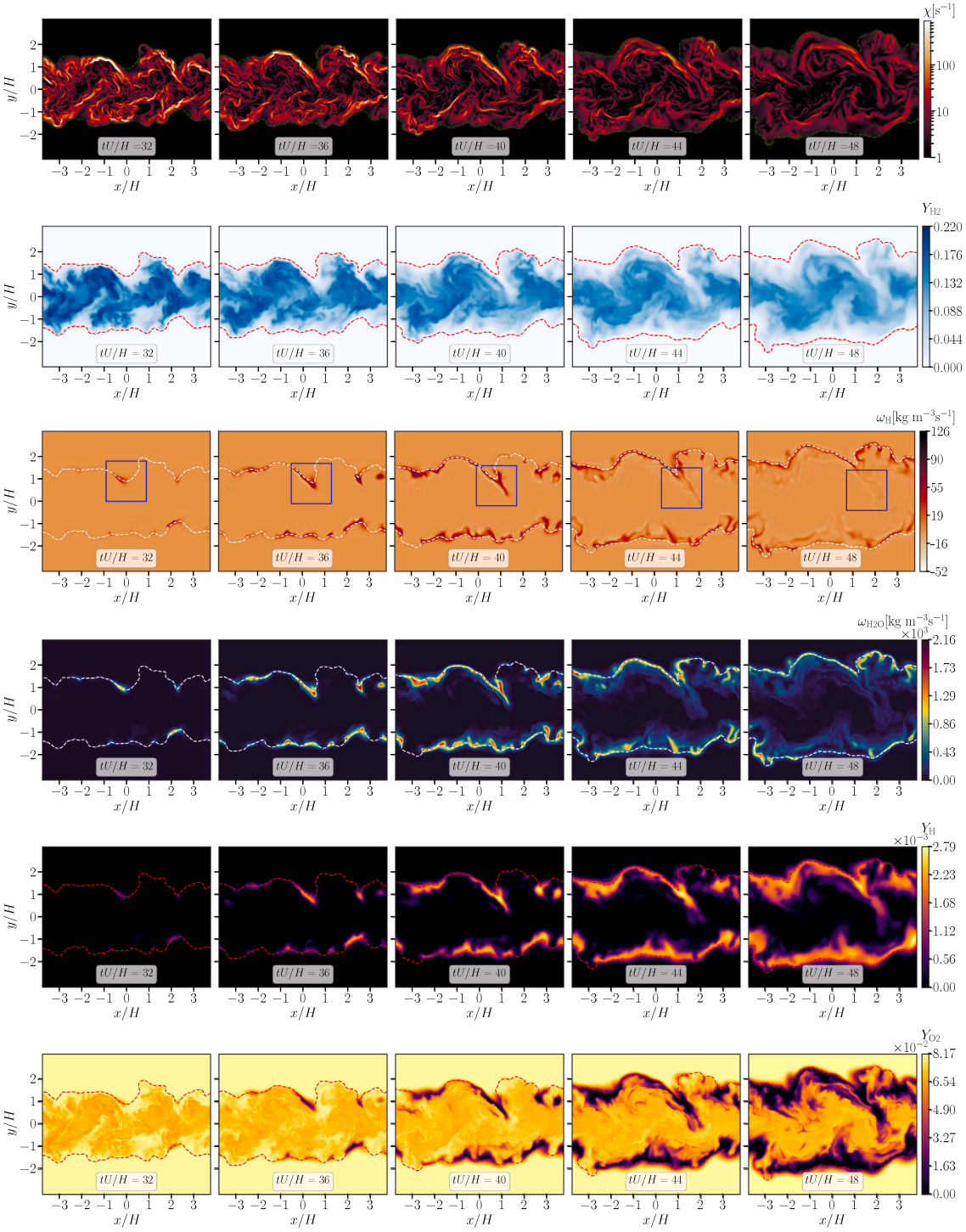

Fig. 3. Evolution of $\chi, Y_H, \omega_H, Y_{H_2O}, Y_{H_2}, Y_{O_2}$ at $t' = [32, 36, 40, 44, 48]$. The common isocontour present in all figures depicts $Z = Z_{st}$ The white isocontours in χ depicts $\chi = 200$ $[1/s]$.

Fig. 6(c) shows the results of conditional average of the chemical source term of water for the JPDF at $t' = 38$ and the FGM. The FGM agrees for the early stage at $Z = Z_{st}$, but it under predicts the later stages, at the scale of 1 standard deviation (σ). For $Z = 2Z_{st}$, the trend is well captured for higher values of progress, but over-predictions occur at the early stage, on a scale slightly larger than 1σ.

5. Considerations for flamelet-based modeling

In the context of turbulent flows, curvature is of utmost importance to predict ignition accurately [17,23], especially when preferential diffusion effects are relevant, as in the case of hydrogen combustion. Preferential diffusion affects the local composition and temperature, which in turn determines the reaction rates. Hence the flamelets used to create the FGM should be chosen in a reliable way. Thus the question addressed here is: which are the most adequate flamelets to represent this case?.

The first type of flamelet studied is the igniting laminar mixing layer (Case $1D_{Le}$), which is the laminar analogue of case $3D_{Le}$. The second type of flamelet is an igniting, curved, and strained counterflow flame, initialized with a mixing solution without chemical reactions. The curved and strained flamelets were computed using Chem1D, varying

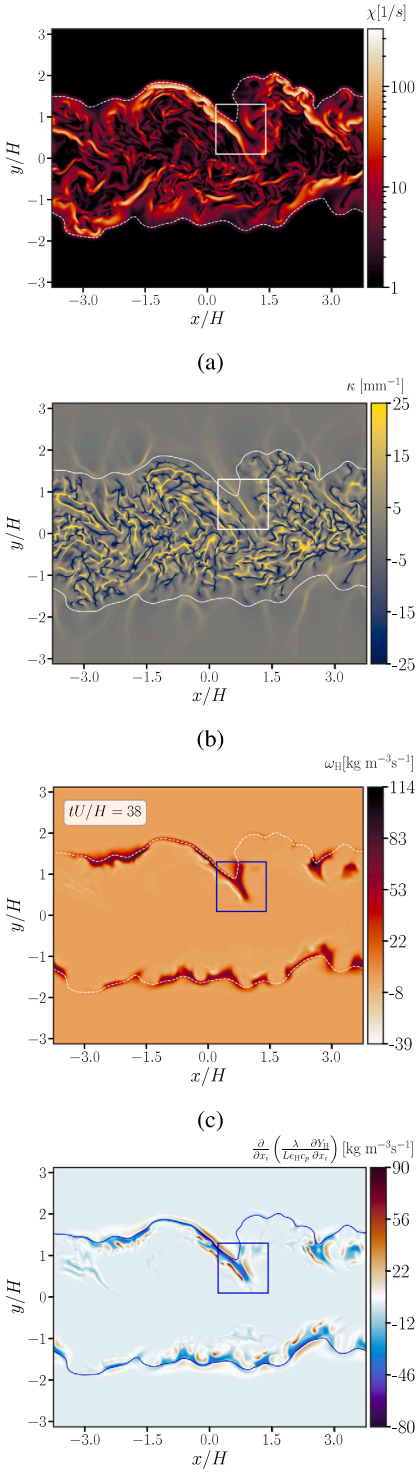

Fig. 4. From top to bottom χ [s^{-1}], κ [mm^{-1}], ω_H [kg $m^{-3}s^{-1}$], Diffusion term [kg $m^{-3}s^{-1}$].

curvature and strain rate (a [s^{-1}]). The range curvature was set to $-10 < \kappa < 10$ mm^{-1} with steps $\Delta\kappa = 1$ mm^{-1} and the range strain rate was set as $100 < a < 1000$ s^{-1} with steps $\Delta a = 100$ s^{-1}. Upon inspection of the flamelets that best enclosed the scatter, small ad-hoc changes in κ and a were made to find even better ones. All flamelets are computed up to a time of $t' = 57$.

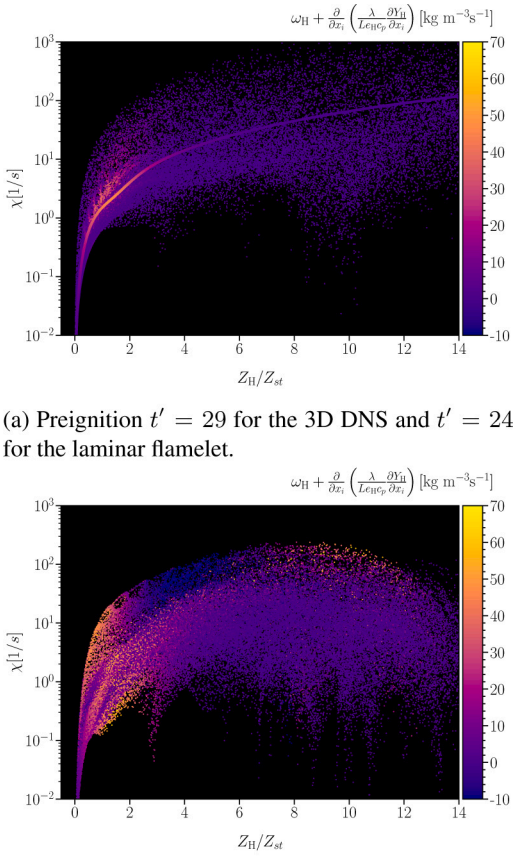

(a) Preignition $t' = 29$ for the 3D DNS and $t' = 24$ for the laminar flamelet.

(b) Extinction, $t' = 38$.

Fig. 5. χ vs Z_H colored by the balance of the radical hydrogen source and diffusion terms.

Attention is devoted to temperature at Z_{st} due to its relevance in applications. Fig. 7 shows the evolution of T vs Y_{H_2O}. The scatter corresponds to data in the middle z-plane from the DNS, the squares are the mean temperature and mean water mass fraction conditioned on $Z = Z_{st}$ at every $\Delta t' = 1$. The lines correspond to the selected flamelets.

The following observations are relevant from Fig. 7: (1) the laminar mixing layer follows the trend of the turbulent case qualitatively. (2) The laminar mixing layer is not capable of enclosing the whole spectrum of scatter, and over-predicts the temperature for advanced progress. (3) The turbulent case shows a remarkable negative correlation which can be seen in the scatter at advanced progress value colored in blue. That means that at advanced progress, the temperature decreases, which should not happen according to flamelet theory when no heat losses are present. (4) Increasing the strainrate with no curvature (CF_1) slightly increases the temperature at the early stage and considerably over predicts temperature and progress for later stages. (5) Moderate strain rate and moderate negative curvature (CF_2) results in a considerably lower temperature with respect to the laminar mixing layer, and can cover the lower part of the scatter. (6) High strainrate and positive curvature (CF_3) will over predict the temperature with respect to the laminar mixing layer, but will be able to cover the upper side of the scatter, however, too high of a strain rate (CF_4) will results a non-monotonical behavior of Y_{H_2O}, which means it can no longer be used to parametrize T, as multiple values would be defined for certain values of Y_{H_2O}.

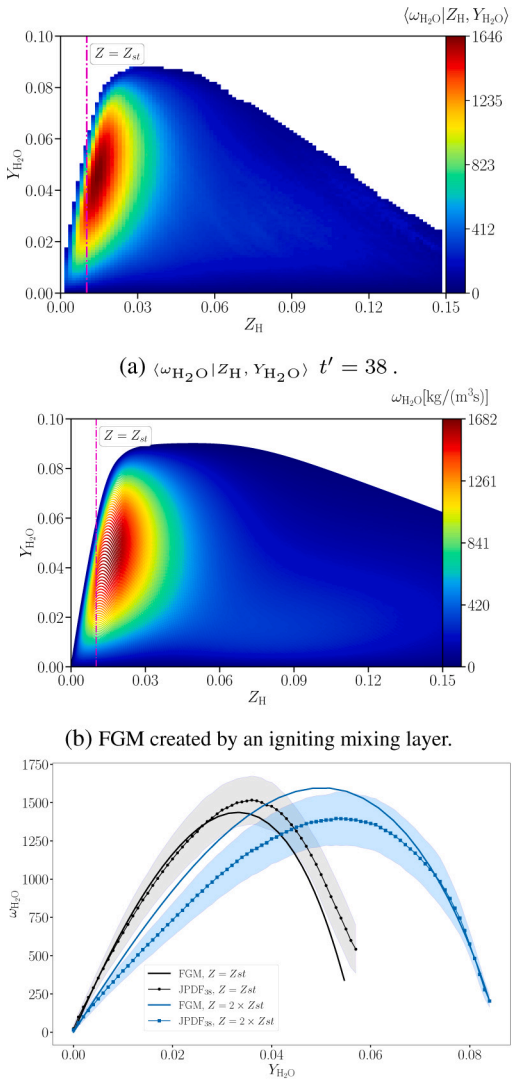

(a) $\langle\omega_{H_2O}|Z_H, Y_{H_2O}\rangle$ $t' = 38$.

(b) FGM created by an igniting mixing layer.

(c) Comparison between the JPDF and FGM conditioned at $Z = Z_{st}$ and $Z = 2Z_{st}$.

Fig. 6. From top to bottom, joint-probability density function of mean water source term conditioned in Z_H, Y_{H_2O}, FGM created by an igniting mixing layer colored by water source term, comparison between the JPDF and the FGM.

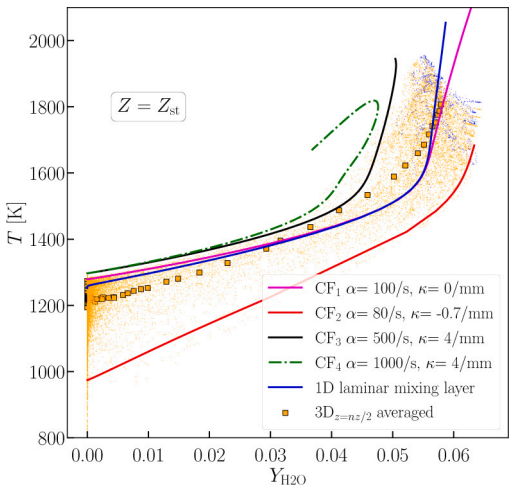

Fig. 7. Evolution of conditioned 3D DNS, 1D mixing-layer and counterflow flames. The blue scatter corresponds to the end time. (For interpretation of the references to color in this figure legend, the reader is referred to the web version of this article.)

6. Conclusions

A temporal, planar, double-shear layer at a $Re = 10\,000$ of pure H_2 surrounded by hot O_2+Ar was computed by means of DNS with detailed chemistry to better understand the ignition process, composition space and flamelet-based modeling, in the context of the Argon Power Cycle. The main conclusions can be summarized as follows:

- Preferential diffusion affects the ignition delay significantly by enhancing the penetration of hydrogen into the oxidizer side. The mechanisms by which turbulence delays ignition are not entirely clear, since lean regions with high scalar dissipation are marked by having high overall production of Y_H, even higher than the laminar flamelet.
- The locations where igniting kernels emerge is characterized by high-scalar dissipation, and convex curvature towards the fuel size. The first aspect goes in contrast to has been reported for other fuels in the literature e.g., [15].
- Curvature effects are key in the development of the igniting kernels, as these show to have an even stronger effect than scalar dissipation, since it can enhance or extinguish these kernels. The reason behind it is attributed to the preferential diffusion of H and H_2, which gets amplified with curvature. This means that ignition does not only depend on high or low levels of scalar dissipation as in other fuels, but also on curvature.
- The mixture fraction and water mass fraction space $(Z, \mathcal{Y})$ created by igniting laminar mixing layers and the one found by the turbulent case during the transition from ignition to quasi-steady state are qualitatively similar, and the FGM created with such flamelets is able to capture the behavior of the water source terms within one standard deviation from the mean in the range of $Z_{st} < Z < 2Z_{st}$ when compared to the joint-probability density function.
- The behavior of temperature versus water is qualitatively captured by the igniting mixing layer, but deviation are observed. Such deviations can be overcome by counterflow flames with varying strain rate and curvature.
- Curvature not only has an effect on the development of igniting kernels but also on the final flames. Curvature enhances the preferential diffusion effects which cause negative correlation between T and Y_{H_2O}.

Novelty and significance statement

The novelty of this research relies, firstly, on the context of the Argon Power Cycle, which has the potential to allow for high efficiency, pollution free combustion of hydrogen. The second novelty of this research relies on the fact that, to the best of our knowledge, this is the first DNS of non-premixed hydrogen combustion in an Argon atmosphere. Furthermore, the turbulent conditions created by the $Re = 10\,000$ allow to study interesting phenomena created by the turbulence-chemistry interaction, like igniting kernel emergence and extinction. Lastly, we find that the laminar mixing layers are qualitatively correct, but not capable of fully representing the composition space created by the turbulent case, and strain rate and curvature are also needed.

CRediT authorship contribution statement

D.A. Quan Reyes: Performed research, Developed analysis tools, Analyzed data, Wrote the paper. **Dirk Roekaerts:** Conceptualized, Analyzed data, Review and editing. **Jeroen van Oijen:** Conceptualized, Designed the research, Managed the project, Acquired funding, Analyzed data, Edited the paper.

Declaration of competing interest

The authors declare that they have no known competing financial interests or personal relationships that could have appeared to influence the work reported in this paper.

Acknowledgments

This work is part of the project Argon Power Cycle with project number 17868 of the Vici research programme, which is (partly) financed by the Dutch Research Council (NWO), The Netherlands. The DNS were performed at the Dutch National Supercomputer Snellius, and the authors thank them for their support.

References

[1] United Nations Environment Program, Emissions Gap Report 2023: Broken Record – Temperatures hit new highs, yet world fails to cut emissions (again) - Executive summary, United Nations Environment Programme, 2023, p. 15.
[2] P.E. Dimotakis, The mixing transition in turbulent flows, J. Fluid Mech. 409 (2000) 69–98.
[3] S.K. Lele, Compact finite difference schemes with spectral-like resolution, J. Comput. Phys. 103 (1) (1992) 16–42.
[4] T.A. Davidson, A simple and accurate method for calculating viscosity of gaseous mixtures, vol. 9456, US Department of the Interior, Bureau of Mines, 1993.
[5] A. Ern, V. Giovangigli, Multicomponent transport algorithms, vol. 24, Springer Science and Business Media, 1994.
[6] M.P. Burke, M. Chaos, Y. Ju, F.L. Dryer, S.J. Klippenstein, Comprehensive H_2 O_2 kinetic model for high-pressure combustion, Int. J. Chem. Kinet. 44 (7) (2011) 444–474.
[7] J.A. van Oijen, Direct numerical simulation of autoigniting mixing layers in MILD combustion, Center for Turbulence Research, Annual Research Briefs (2011).
[8] A. Coussement, O. Gicquel, J. Caudal, B. Fiorina, G. Degrez, Three-dimensional boundary conditions for numerical simulations of reactive compressible flows with complex thermochemistry, J. Comput. Phys. 231 (2012).
[9] T.J. Poinsot, S.K. Lele, Boundary conditions for direct simulations of compressible viscous flows, J. Comput. Phys. 101 (1) (1992) 104–129.
[10] G. Lodato, Tridimensional Boundary Conditions for Direct and Large-Eddy Simulation of Turbulent Flows. Sub-Grid Scale Modeling for Near-Wall Region Turbulence (Ph.D. thesis), Institut National des Sciences Appliqueees de Rouen, 2011.
[11] J.C. Sutherland, C.A. Kennedy, Improved boundary conditions for viscous, reacting, compressible flows, J. Comput. Phys. 191 (2) (2003) 502–524.
[12] G.B. Skinner, G.H. Ringrose, Ignition delays of a hydrogen-oxygen-argon mixture at relatively low temperatures, J. Chem. Phys. 42 (6) (1965) 2191–2192.
[13] T. Kathrotia, M. Fikri, M. Bozkurt, M. Hartmann, U. Riedel, C. Schulz, Study of the H+O+M reaction forming OH(star): Kinetics of OH* chemiluminescence in hydrogen combustion systems, Combust. Flame 157 (7) (2010) 1261–1273.
[14] A.A. Konnov, Yet another kinetic mechanism for hydrogen combustion, Combust. Flame 203 (2019) 14–22.
[15] E. Mastorakos, Ignition of turbulent non-premixed flames, Prog. Energy Combust. Sci. 35 (1) (2009) 57–97.
[16] J.A. Van Oijen, Direct numerical simulation of autoigniting mixing layers in MILD combustion, Proc. Combust. Inst. 34 (1) (2013) 1163–1171.
[17] M.U. Göktolga, J.A. van Oijen, L.P.H. de Goey, 3D DNS of MILD combustion: A detailed analysis of heat loss effects, preferential diffusion, and flame formation mechanisms, Fuel 159 (2015) 784–795.
[18] C.K. Law, Combust. Phys., Cambridge University Press, 2006, p. 714.
[19] J. Van Oijen, L. de Goey, Modelling of premixed laminar flames using flamelet-generated manifolds, CST 161 (1) (2000) 113–137.
[20] S. Delhaye, L.M. Somers, J.A. van Oijen, L.P. de Goey, Incorporating unsteady flow-effects in flamelet-generated manifolds, Combust. Flame 155 (1–2) (2008) 133–144.
[21] L.M. Verhoeven, W.J. Ramaekers, J.A. van Oijen, L.P. de Goey, Modeling non-premixed laminar co-flow flames using flamelet-generated manifolds, Combust. Flame 159 (1) (2012) 230–241.
[22] J. van Oijen, A. Donini, R. Bastiaans, J. ten Thije Boonkkamp, L. de Goey, State-of-the-art in premixed combustion modeling using flamelet generated manifolds, Prog. Energy Combust. Sci. 57 (2016) 30–74.
[23] M.U. Göktolga, L.P.H. de Goey, J.A. van Oijen, Modeling curvature effects in turbulent autoigniting non-premixed flames using tabulated chemistry, Proc. Combust. Inst. 38 (2) (2021) 2741–2748.